LETTER

Tunable acoustic absorbers with periodical micro-perforations having varying pore shapes

A Letters Journal Exploring the Frontiers of Physics

November 2017

EPL, **120** (2017) 44001
doi: 10.1209/0295-5075/120/44001

www.epljournal.org

Tunable acoustic absorbers with periodical micro-perforations having varying pore shapes

Shuwei Ren[1,2], Xuewei Liu[1,2], Junqing Gong[1,2], Yufan Tang[1,2], Fengxian Xin[1,2(a)], Lixi Huang[3] and Tian Jian Lu[1,2]

[1] *MOE Key Laboratory for Multifunctional Materials and Structures, Xi'an Jiaotong University - Xi'an 710049, PRC*
[2] *State Key Laboratory for Strength and Vibration of Mechanical Structures, Xi'an Jiaotong University Xi'an 710049, PRC*
[3] *Department of Mechanical Engineering, The University of Hong Kong - Pokfulam Road, Hong Kong*

received 11 September 2017; accepted in final form 10 January 2018
published online 5 February 2018

PACS 43.20.-f – General linear acoustics
PACS 43.20.Hq – Velocity and attenuation of acoustic waves

Abstract – Circular pores with sub-millimeter diameters have been widely used to construct micro-perforated panels (MPPs), the acoustical performance of which can be predicted well using the Maa theory (Maa D.-Y., *J. Acoust. Soc. Am.*, **104** (1998) 2861). We present a tunable MPP absorber with periodically arranged cylindrical pores, with their cross-sectional shapes systematically altered around the circle while maintaining their cross-sectional areas unchanged. Numerical analyses based on the viscous-thermal coupled acoustical equations are utilized to investigate the tunable acoustic performance of the proposed absorbers and to reveal the underlying physical mechanisms. We demonstrate that pore morphology significantly affects the sound absorbption of MPPs by modifying the velocity field (and hence viscous dissipation) in the pores. Pore shapes featured as meso-scale circular pores accompanied with micro-scale bulges along the boundaries can lead to perfect sound absorption at relatively low frequencies. This work not only enriches the classical Maa theory on MPPs having circular perforations, but it also opens a new avenue for designing subwavelength acoustic metamaterials of superior sound absorption in target frequency ranges.

Introduction. – Sound absorbing materials/structures (SAM/S) with tunable functioning frequency range that target a variety of working situations have been pursued for decades. When the surface impedance of SAM/S in a certain frequency range is modified to well match the characteristic impedance of the medium in which sound wave is propagating, the kinetic and potential energy of the sound wave are mostly absorbed. For the passive category of SAM/S, such as porous materials [1–6], the working frequency range has been adjusted mainly by changing the material thickness according to quarter-wavelength resonance, as well as by changing the pore size and porosity (so as to alter the permeability). Recently, numerous acoustic-dissipating metamaterials were designed by manipulating with local-resonances [7–9], anisotropic equivalent properties [10–13], the scalar field nature of the sound wave [14,15], acoustic coherence [16,17], and sonic crystals [18,19]. The operating frequency range can be tuned by modifying the internal micro-structures of these metal materials. A micro-perforated panel (MPP), as a typical SAM/S, is composed of a thin panel having periodically arranged circular micro-perforations that is backed with a cavity. Figure 1(a) presents the lateral view of a classical MPP. When a sound wave impinges upon the MPP, a part of it penetrates into the panel and is dissipated inside the micro-perforations.

In the current study, based on conventional MPPs having circular perforations, we present a category of tunable acoustic meta-absorbers consisting of thin panels that contain non-circular perforations. By systematically varying the pore shape, the surface impedance of the proposed MPP is altered, enabling broadband sound absorption with adjusting working frequency range.

Beyond the regular pore shape of a circle, the non-circular pores considered in the present study are sketched as fig. 1(b), the shapes of which are controlled by two

(a)E-mail: fengxian.xin@gmail.com

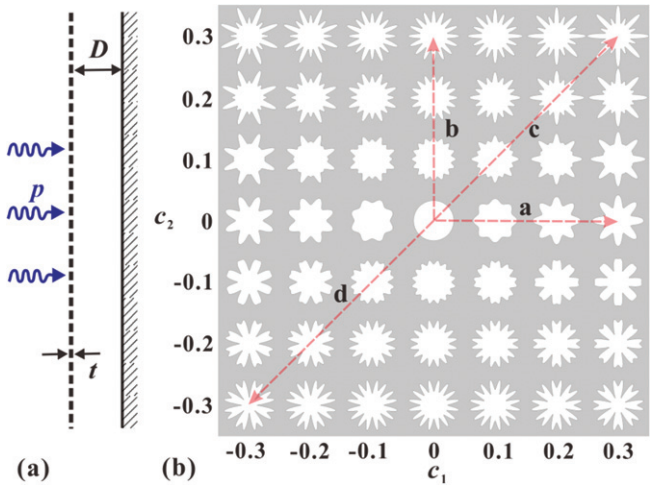

Fig. 1: (Color online) (a) Lateral view of a classical MPP and (b) typical pore shapes controlled by the two shape parameters c_1 and c_2, with red dashed lines indicating the four main varying paths.

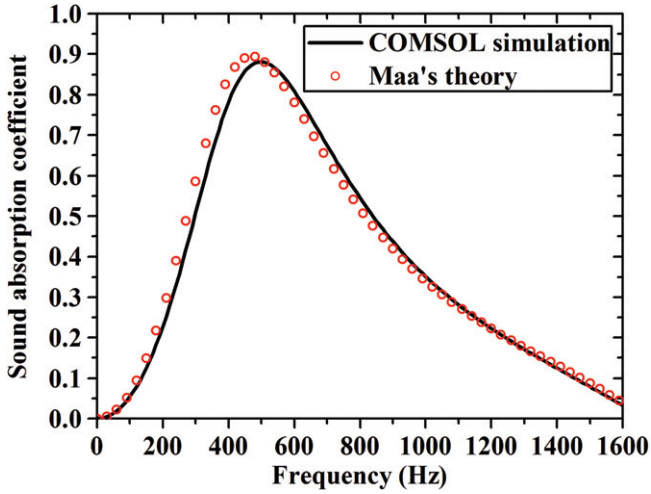

Fig. 2: (Color online) Validation through comparing numerical simulation results with the predicted results by Maa's theoretical model (the MPP is designed with $d = 0.4\,\text{mm}$, $t = 0.5\,\text{mm}$, $\sigma = 1\%$, and $D = 100\,\text{mm}$).

shape parameters (c_1 and c_2). Upon varying c_1 and c_2 in the range from -0.3 to 0.3, the pore shapes are seen to vary periodically. The varying pore shapes are expected to provide more acoustic tunability than the circular pores. To specify the effects of the pore shape, let the pore morphologies of fig. 1(b) be expressed as $x = r(\theta)\cos\theta$ and $y = r(\theta)\sin\theta$, in which

$$r(\theta) = r_0[1 + c_1\cos(8\theta) + c_2\cos(16\theta)], \tag{1}$$

where x and y are the horizontal and vertical coordinates of the periphery line, respectively. Meanwhile, $r(\theta)$ is the altering radius formed as the Taylor series, and r_0 is the fundamental radius which, for the purpose of sound absorption, is equal to a sub-millimeter. θ is required to vary from 0 to 2π, thus the peripheries can form closed loops. It can be seen that the pores are eightfold symmetrical, and the amplitude of the pore periphery increases with the absolute value of c_1 and/or c_2. Therefore, this class of pore shapes provides sufficient variation ranges to study pore shape effects on the acoustical performance of MPPs. It should be noted that for sound incidence in the normal direction, the pores distributed symmetrically about the axis of $c_1 = 0$ are regarded as the same ones, just with a $\pi/8$ phase difference. For simplicity, the pores of the proposed MPPs are arranged in a square array, with L_0 representing the center-to-center distance between neighboring pores. Hence, r_0 can be calculated as

$$r_0 = \frac{L_0\sqrt{2\sigma}}{\sqrt{\pi\,(2 + c_1^2 + c_2^2)}} \tag{2}$$

in which σ is the perforation ratio. Conveniently, the cross-sectional areas of the pores remain unchanged if L_0 and σ are fixed. Consequently, pores with identical cross-sectional areas but periodically varying shapes can be obtained. As the shape parameters c_1 and c_2 can both be valued as real numbers that vary continuously in a one-dimensional space, the pore shape can be modified continuously in a two-dimensional space, with space boundaries as $0 \le x \le L_0/2$ and $0 \le y \le L_0/2$.

Theory. – Physically, sound absorption in a MPP is mainly contributed by friction (viscous) dissipation [20,21] within the boundary layers inside the pores, as well as around the inlet and outlet of the pores. Moreover, through electro-acoustical analogy (for example, the cross-sectional average velocity inside a pore corresponds to the electric current), the MPPs can be regarded as boundaries characterized with acoustical resistance and reactance. Particularly, when both c_1 and c_2 equal 0, the pore shape is a circle (in the center of fig. 1(b)) so that the acoustical resistance and reactance can be predicted well by Maa's theory [22] as

$$r + i\omega m = \frac{i\omega t}{\sigma c_0}\left[1 - \frac{2}{k\sqrt{-i}}\frac{J_1\left(k\sqrt{-i}\right)}{J_0\left(k\sqrt{-i}\right)}\right]^{-1} + \frac{\sqrt{2}\eta k}{\sigma\rho_0 c_0 d} + i\frac{0.85\omega d}{\sigma c_0}. \tag{3}$$

Here, $k = d\sqrt{\omega\rho_0/4\eta}$ is a dimensionless factor indicating the ratio of pore size to viscous boundary thickness, J_1 is the Bessel function of the first kind and the first order, J_0 is the Bessel function of the first kind and the zeroth order, d is the pore diameter, t is the panel thickness, η is the dynamic viscosity of air, ρ_0 is the density of air, c_0 is the sound speed in air, and ω is the angular frequency of impinging sound wave. The acoustical reactance is the product of ω and the acoustical mass m. The last terms on the right-hand side of eq. (3) are the end corrections,

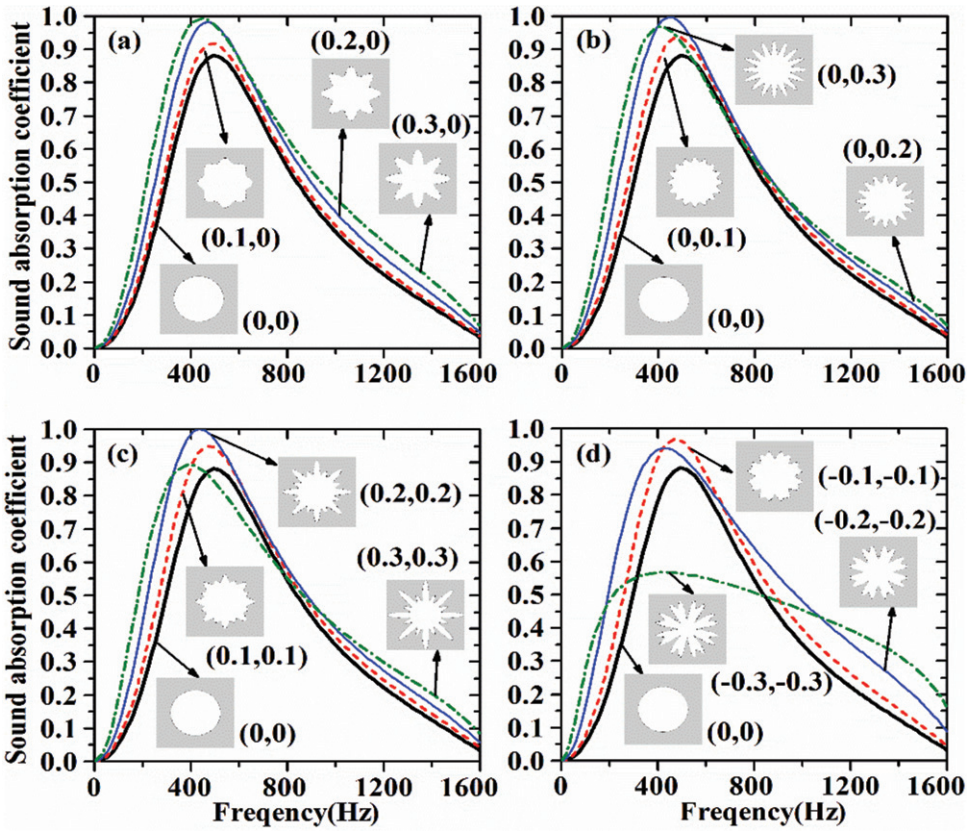

Fig. 3: (Color online) Influence of the pore shape on the sound absorption coefficient, as a function of frequency ($0 \sim 1600\,\mathrm{Hz}$), for MPPs with identical cross-sectional area: numbers in brackets stand for (c_1, c_2), and the label characters in the sub-figures correspond to the path characters in fig. 1(b).

corresponding to sound dissipation and sound radiation around the inlet and outlet, respectively.

The back cavity in the MPP absorber is modeled as pure acoustic reactance, since no energy consumption takes place there, as

$$Z_D = -i\rho_0 c_0 \cot(\omega D/c_0) \tag{4}$$

in which D is the cavity depth. With determined acoustical resistance and reactance, the sound absorption coefficient of the MPP can be expressed as

$$\alpha = \frac{4r}{(r+1)^2 + (\omega m - \cot(\omega D/c_0))^2}. \tag{5}$$

The maximum value of sound absorption, $\alpha = 4r/(r+1)^2$, is achieved when the acoustic reactance match (resonant state) occurs, namely $\omega m - \cot(\omega D/c_0) = 0$: that is, the reactance provided by the pore is compensated by that offered by the back cavity. Further, if the acoustic resistance of the structure matches that of air ($\rho_0 c_0$) simultaneously, namely $r = 1$, perfect sound absorption (α =1) is achieved.

Numerical results and comparison. – Even though the acoustical reactance of the back cavity defined by eq. (4) as well as the relation between the sound absorption coefficient and acoustical resistance and reactance as expressed by eq. (5) are feasible for MPPs having different pore shapes under normal sound incidences, the acoustical resistance and reactance of the periodically varying pores studied here are difficult to model theoretically. Instead, the acoustical properties of these irregular pores are obtained by numerically calculating the viscous-thermal-coupled acoustical equations. Simulation models are built in the preset module Thermoacoustics of COMSOL, where the viscosity and thermal conduction of air are taken into consideration via no-slip and isothermal boundary conditions, respectively. Given the periodicity of the pores, only one-fourth of a unit cell containing one pore and the corresponding incidence part and back cavity is sufficient to model the whole MPP structure. Only the fluid regions (air) with symmetrical boundaries are created, and sound-hard boundaries are imposed on the interfaces between air and the MPP, because the fluid-solid coupling effect is ignored. In order to fully capture the influence of viscous and thermal boundary layers, the smallest mesh size inside the micro-perforations and adjacent to the perforation walls is smaller than the thickness of the viscous boundary layer at the highest frequency (1600 Hz). Moreover, quadratic elements are used. It has been established that the calculation convergence is guaranteed. The properties of air are settled as density $\rho_0 = 1.21\,\mathrm{kg/m^3}$, sound speed $c_0 = 343\,\mathrm{m/s}$, and dynamic viscosity

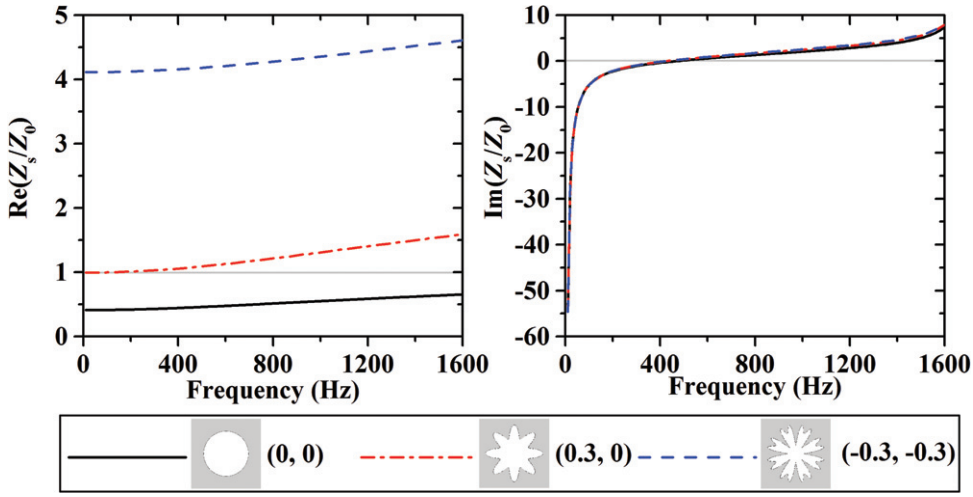

Fig. 4: (Color online) Real (surface acoustic resistance) and imaginary (surface acoustic reactance) parts of normalized surface impedance.

$\eta = 1.56 \times 10^{-5}$ Pa s. With a normal incidence plane wave with amplitude 1 Pa impinging on the front surface of the MPP, the velocity and pressure field are determined accordingly. The surface impedance Z_s of the structure can be extracted by calculating the ratio of average sound pressure to average particle velocity at the surface. Finally, the sound absorption coefficient is calculated via $\alpha = 1 - (|Z_s - \rho_0 c_0|/|Z_s + \rho_0 c_0|)^2$.

To validate the simulation model, the sound absorption coefficient of a classical MPP with circular pores ($d = 0.4$ mm, $\sigma = 1\%$, $t = 0.5$ mm and $D = 100$ mm) obtained by COMSOL simulation is first compared with that predicted by Maa's model in fig. 2. The corresponding parameters of the periodically varying pores are $L_0 = 3.55$ mm, $\sigma = 1\%$, $c_1 = 0$, and $c_2 = 0$. While overall good agreement is achieved, relatively small discrepancies do exist, which mainly stem from the neglect of thermal dissipation in Maa's model, as well as from its simplified approximation towards the acoustic resistance and reactance end effects.

Next, we quantify numerically the influence of the pore shape on the sound absorption capacity of a MPP. Figure 3 presents the sound absorption curves corresponding to four representative paths, with the basic parameters fixed as $L_0 = 3.55$ mm, $\sigma = 1\%$, $t = 0.5$ mm and $D = 100$ mm. It is well known that, for MPPs, the curve dips are dominated by the extra reactance coming from the back cavity. That is, when $\omega D/c_0 = n\pi$ ($n = 0, 1, 2, \ldots$), Z_D of eq. (4) approaches infinity and thus α approaches 0 via eq. (5). Accordingly, the first dips on these curves are located at around 1715 Hz, which is beyond the upper limit (1600 Hz) of the studied frequency range in fig. 3. In contrast, the curve peaks are determined by the impedance of both the pores and the back cavity. Specifically, because the resistance is merely derived from the pores, the pore shape has significant influence on these peaks.

As shown in figs. 3(a) and (b), along the horizontal ($c_2 = 0$) and vertical ($c_1 = 0$) axes in fig. 1(b), the pore

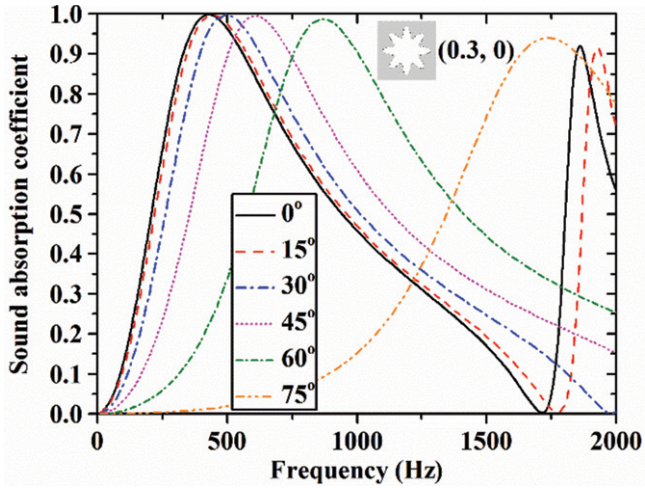

Fig. 5: (Color online) Influence of the incidence angle on the sound absorption coefficient plotted as a function of frequency ($0 \sim 2000$ Hz) for MPP with pore shape (0.3, 0).

shape varies from a circle to a gear-like appearance. As c_1 is increased, the amplitude of boundary variation is enhanced, giving rise to the elevation of absorption peaks, the broadening of the band width, and the slight left-shift of the peak frequencies (fig. 3(a)). For the pore with shape (0.3, 0), its absorption peak approaches 1, where total absorption takes place. Comparatively, the number of "gear-teeth" of the pores in fig. 3(b) is twice that in fig. 3(a), which is determined by the periodic parameters within the cosine functions of eq. (1). In general, the more intense distribution of "gear-teeth" is seen to cause an earlier arising of the absorption curve towards perfect absorption, *e.g.*, pore shape (0, 0.2) in fig. 3(b). On the contrary, an exceeding variation of the pore periphery such as pore shape (0, 0.3) leads to deteriorated sound absorption. Due to the dissimilarity of the periods of the cosine functions corresponding to c_1 and c_2, the

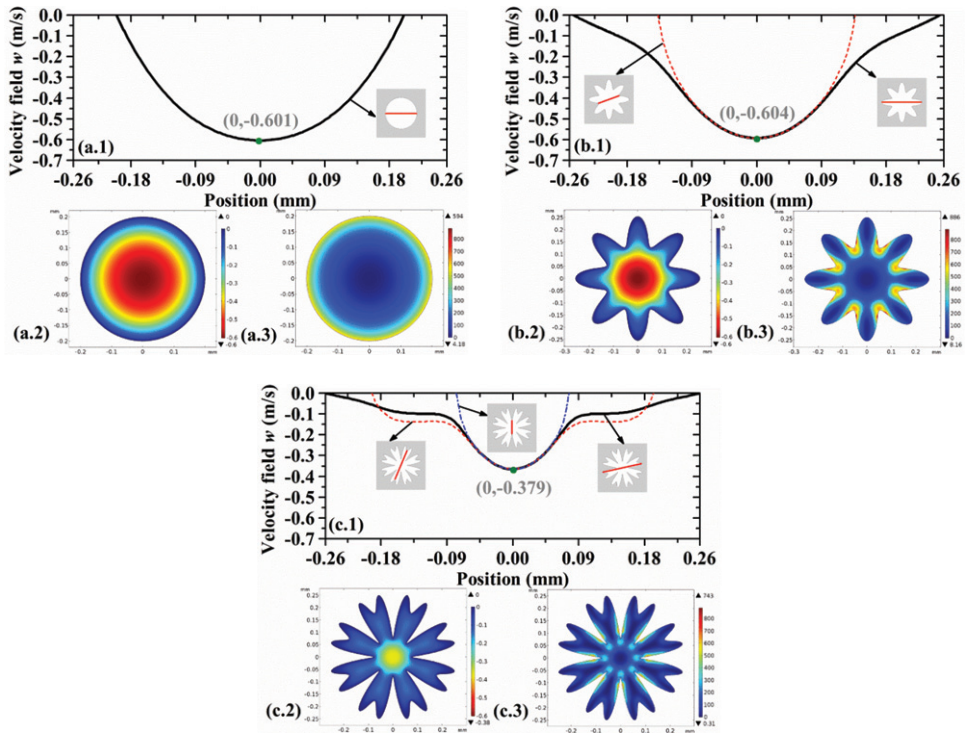

Fig. 6: (Color online) (a.1), (b.1), (c.1): velocity distribution in selected pores. (a.2), (b.2), (c.2): velocity distribution on pore cross-section at half pore thickness. (a.3), (b.3), (c.3): sound energy dissipation density ($\mathrm{W/m^3}$) on pore cross-section at half pore thickness. All quantities are calculated at 500 Hz.

amplitudes of the pore boundary variation in fig. 3(c) are not uniform, yet still periodical. These pore shapes appear like snowflakes. However, the variation trend of the absorption curve with varying pore shape is highly similar to that in fig. 3(b), attributed to the comparable size and distribution of boundary variations in figs. 3(b) and (c). As to the varying path in fig. 3(d), the pore boundary fluctuates so dramatically that the pore with shape (−0.3, −0.3) has no apparent circle-like main pore at its center, thus causing the earlier weakening of its absorption curve. Nevertheless, the band width of pore shape (−0.3, −0.3) is expanded tremendously.

Physical mechanisms. – To reveal the physical mechanisms underlying the effects of the pore shape on sound absorption, we first evaluate the mesoscopic characterization (*i.e.*, normalized surface impedance) of pore shapes, which is related to pore morphology, perforation ratio, panel thickness and cavity depth. The normalized surface acoustic resistance and reactance correspond to r and $\omega m - \cot(\omega D/c_0)$ of eq. (5), respectively. Without losing generality, three representative pore shapes, (0, 0), (0.3, 0) and (−0.3, −0.3), are analyzed, as shown in fig. 4, using the experiment-like method [23]. More specifically, with the velocity and pressure field calculated for a pore backed with cavity, the surface impedance can be extracted through $Z_\mathrm{s} = \langle p\rangle_\mathrm{inlet}/\langle v\rangle_\mathrm{inlet}$. Here, $\langle\cdot\rangle$ denotes the average calculation on a specific surface. It can be seen from fig. 4 that the pore shape significantly affects the acoustic resistance but not so much the acoustic reactance. In particular, the acoustic resistance of the pore with shape (−0.3, −0.3) is the largest, resulting in severer impedance mismatch with that of air. Correspondingly, this pore shape has the poorest sound absorption capability. Nonetheless, it should be noted that, for the circular pore (0, 0), insufficient acoustic resistance also leads to impedance mismatch. Consequently, only a proper pore shape, *e.g.*, (0.3, 0), with pertinent acoustic resistance can reach perfect sound absorption.

Another important inspiration from fig. 4 is that the perfect sound absorption of pore shape (0.3, 0) is quasi-omnidirectional, as shown in fig. 5. For oblique sound incidence with an angle ϕ to the normal direction, the acoustic impedance $r + i\omega m$ of the perforated panel itself remains unchanged. However, the acoustic reactance of the back cavity is changed as $Z'_D = -i\rho_0 c_0 \cot(\omega D\cos\phi/c_0)/\cos\phi$, due to the difference in sound traveling path [22]. Therefore, the condition for absorption peaks is evolved as $\omega m\cos\phi - \cot(\omega D\cos\phi/c_0) = 0$. In other words, the peak frequency under oblique incidence will move to higher frequency compared to that under normal incidence. Further, as the acoustic resistance of the pore with shape (0.3, 0) is close to 1 in a relatively wide frequency range (fig. 4), the peak value decreases sluggishly with the movement of peak frequencies. Besides, in a diffusive field, the absorption band of a MPP with pore shape (0.3, 0) will extend continually to higher frequency and become broadened [22], compared to that in a normal field. The sound

absorption coefficient can maintain a high value (close to 1), due to this quasi-omnidirectional perfect absorption behavior.

We also thoroughly examine the pore shape effects from a microscopic perspective, in view of velocity and sound energy dissipation distributions within the pore as illustrated in fig. 6. The dissipation of the sound energy in fig. 6 is only contributed by air viscosity, because for MPPs it has been established that thermal dissipation is negligible. Physically, viscous dissipation is directly related to the velocity field in the pore. From figs. 6(a.2), (b.2), (c.2), it is found that the distribution of air particle velocity inside the pore is remarkably dependent upon the pore shape, causing the huge difference among the distributions of dissipation density in the three pores considered (figs. 6(a.3), (b.3), (c.3)). In particular, for the pore of shape (0.3, 0), the velocity pattern at its central section is comparable to that in the circular pore, with similar extreme values (figs. 6(a.1), (b.1)). Further, the enhanced velocity gradient in the central area of the pore with shape (0.3, 0) causes more energy dissipation, finally leading to perfect sound absorption. In sharp contrast, not only the amplitude of velocity in the pore of shape $(-0.3, -0.3)$ decreases evidently compared to that in the circular pore, but also flat velocity distribution with little gradient appears diffusely (fig. 6(c.1)), causing eventually inferior sound absorption.

Summary and conclusion. – A type of tunable MPPs containing periodically distributed microperforations with varying pore morphologies had been designed and characterized using numerical simulations. It was demonstrated that the pore shape affects significantly the sound absorption behavior of the MPP. While pore shapes featured as meso-scale circular main-pores accompanied with micro-scale bulges along the boundaries could lead to perfect sound absorption, pore shapes featured mainly as narrow micro-scale slits could also deteriorate the absorption performance. Physical mechanisms underlying such pore shape effects were explored from both mesoscopic and microscopic viewpoints. The results obtained in this study enable designing high-performance MPPs for low-frequency sound absorption.

* * *

This work was supported by the National Natural Science Foundation of China (11761131003, U1737107, 51528501 and 11772248) and the Shannxi Foundation for Selected Overseas Chinese (2017025).

REFERENCES

[1] Allard J. F. and Atalla N., *Propagation of Sound in Porous Media: Modelling Sound Absorbing Materials* (John Wiley & Sons, United Kingdom) 2009.
[2] Yang X. H., Ren S. W., Wang W. B., Liu X., Xin F. X. and Lu T. J., *Compos. Sci. Technol.*, **118** (2015) 276.
[3] Meng H., Ao Q. B., Ren S. W., Xin F. X., Tang H. P. and Lu T. J., *Compos. Sci. Technol.*, **107** (2015) 10.
[4] Perrot C., Chevillotte F. and Panneton R., *J. Acoust. Soc. Am.*, **124** (2008) 940.
[5] Perrot C., Chevillotte F., Hoang M. T., Bonnet G., Becot F. X., Gautron L. and Duval A., *J. Appl. Phys.*, **111** (2012) 014911.
[6] Chevillotte F., Perrot C. and Guillon E., *J. Acoust. Soc. Am.*, **134** (2013) 4681.
[7] Mei J., Ma G., Yang M., Yang Z., Wen W. and Sheng P., *Nat. Commun.*, **3** (2012) 756.
[8] Fink M., *Nat. Mater.*, **13** (2014) 848.
[9] Jiang H. and Wang Y., *J. Acoust. Soc. Am.*, **132** (2012) 694.
[10] Li R.-Q., Zhu X.-F., Liang B., Li Y., Zou X.-Y. and Cheng J.-C., *Appl. Phys. Lett.*, **99** (2011) 193507.
[11] Gu Z.-m., Liang B., Li Y., Zou X.-y., Yin L.-l. and Cheng J.-c., *J. Appl. Phys.*, **117** (2015) 074502.
[12] Climente A., Torrent D. and Sanchez-Dehesa J., *Appl. Phys. Lett.*, **100** (2012) 144103.
[13] Zheng L.-Y., Wu Y., Zhang X.-L., Ni X., Chen Z.-G., Lu M.-H. and Chen Y.-F., *AIP Adv.*, **3** (2013) 102122.
[14] Cai X., Guo Q., Hu G. and Yang J., *Appl. Phys. Lett.*, **105** (2014) 121901.
[15] Li Y. and Assouar B. M., *Appl. Phys. Lett.*, **108** (2016) 063502.
[16] Wei P., Croënne C., Tak Chu S. and Li J., *Appl. Phys. Lett.*, **104** (2014) 121902.
[17] Song J. Z., Bai P., Hang Z. H. and Lai Y., *New J. Phys.*, **16** (2014) 033026.
[18] Garcia-Chocano V. M., Cabrera S. and Sánchez-Dehesa J., *Appl. Phys. Lett.*, **101** (2012) 184101.
[19] Guild M. D., García-Chocano V. M., Kan W. and Sánchez-Dehesa J., *J. Appl. Phys.*, **117** (2015) 114902.
[20] Azma S., Rezazadeh G., Shabani R. and Alizadeh-Haghighi E., *Acta Mech. Sin.*, **32** (2016) 397.
[21] Peng Z., Pak O. S., Feng Z., Liu A. P. and Young Y.-N., *Acta Mech. Sin.*, **32** (2016) 1012.
[22] Maa D.-Y., *J. Acoust. Soc. Am.*, **104** (1998) 2861.
[23] Ren S. W., Meng H., Xin F. X. and Lu T. J., *J. Appl. Phys.*, **119** (2016) 014901.